Clays and Clay Minerals, Vol. 59, No. 5, 478–489, 2011.

VOLCANISM IN ASSOCIATION WITH THE PRELUDE TO MASS EXTINCTION AND ENVIRONMENT CHANGE ACROSS THE PERMIAN-TRIASSIC BOUNDARY (PTB), SOUTHERN CHINA

HANLIE HONG*, SHUCHENG XIE, AND XULONG LAI

State Key Laboratory of Geological Process and Mineral Resources, China University of Geosciences, Wuhan, Hubei, 430074, P.R. China

Abstract—In order to better understand the provenance of the sediments and environmental change associated with the Permian-Triassic (P/T) biotic crisis, a comparative clay mineralogical study of the Permian-Triassic boundary (PTB) sediments between the Meishan section (the Global Stratotype Section and Point of the PTB) and the Xiakou section, southern China, was undertaken using X-ray diffraction and differential scanning calorimetry (DSC). The results showed that clay minerals of the packstone bed 24e, in which the preludial mass extinction occurred at Meishan, consist of 56% mixed-layer illite-smectite (I-S), 39% illite, and 5% kaolinite. A dehydroxylation effect was measured at 652ºC, indicating that I-S and illite of this bed contain mainly *cis*-vacant (*cv*) layers related to volcanic origin. The dehydroxylation event correlates with bed P257 at Xiakou. The white clay bed 25 also corresponding to the main extinction event at Meishan contains 95% I-S and 5% kaolinite, with a strong endothermic effect at 676ºC and a weaker one at 514ºC in the DSC curve. These results are attributed to dehydroxylation of *cv* layers in I-S clays, suggesting that I-S in the white clay bed was derived from marine alteration of volcanic ash, in agreement with the conodont-correlated clay (P258) at Xiakou. (Conodonts are tooth-like microfossils and are usually used as an indicator of age in PTB stratigraphy.) Increases in chlorite and illite contents in the black clays (bed 26) at Meishan and the conodont-correlated black clay layer (P259b) at Xiakou probably indicate stronger erosional processes under cooler and more arid conditions. Volcanic materials found in a bed which marked the prelude to the main episode of mass extinction reinforce the temporal link between volcanism and the mass extinction.

Key Words—Mixed-layer Illite-smectite (I-S) Clays, Permian-Triassic Boundary (PTB), Preludial Mass Extinction, Volcanism.

INTRODUCTION

The mass extinction at the Permian-Triassic boundary (PTB) has been recognized as the most serious biotic crisis in the history of life, in which both marine and terrestrial biota suffered near annihilation (Erwin, 1994; Jin *et al*., 2000). Proposed catastrophic hypotheses for the extinction event include bolide impact (Becker *et al*., 2001; Basu *et al*., 2003), oceanic anoxia (Wignall *et al*., 1998; Meyer *et al*., 2008; Grasby and Beauchamp, 2009), volcanism (Renne *et al*., 1995; Courtillot and Olson, 2007), a greenhouse event (Retallack, 2001; Kidder and Worsley, 2003), H_2S poisoning (Kump *et al*., 2005), release of methane gas hydrates flooding the world's atmosphere with methane (de Wit *et al*., 2002; Heydari and Hassanzadeh, 2003; Sheldon, 2006), sea-level rise (Hallam and Wignall, 1999), or some synergistic combination of these (Hallam and Wignall, 1997; Knoll *et al*., 2007; Korte and Kozur, 2010). Even though the causes of these disturbances are still debated, the identification of a pronounced and worldwide negative carbon isotope excursion at the PTB suggests a strong disruption in carbon reservoirs (Holser *et al*., 1989; Jin *et al*., 2000), probably related to prominent volcanic events at the Siberian Traps (Wignall, 2001; Knoll *et al*., 2007; Xie *et al*., 2007; Korte and Kozur, 2010).

Recent studies of PTB stratigraphic sets in southern China confirm that the biotic crisis experienced multiple pulses of extinction (Xie *et al*., 2007; Yin *et al*., 2007a). The Global Stratotype Section and Point (GSSP) of the PTB was established and ratified by the International Union of Geological Sciences (IUGS) at Section D, Meishan, Changxing County, Zhejiang Province, southern China (Figure 1; Yin *et al*., 2001). The regional strata in Meishan area include marine Silurian to Lower Triassic rocks, terrestrial Jurassic and Quaternary strata, and the Meishan P/T succession, consisting of the Changhsing Formation in the lower part and the Yinkeng Formation in the upper part (Figure 2). Bed 24e (10 cm thick) consists of dark gray bioclastic packstone, which is within the uppermost portion of the Changhsing Formation. The overlying bed 25 (4 cm thick) is a light bluish gray clay and bed 26 (6 cm thick) is a dark gray clay. Bed 27 (16 cm thick) is a light yellow marl and the P/T boundary was placed in the middle of this bed. The overlying bed 28 (4 cm thick) is

* E-mail address of corresponding author:
honghl8311@yahoo.com.cn
DOI: 10.1346/CCMN.2011.0590505

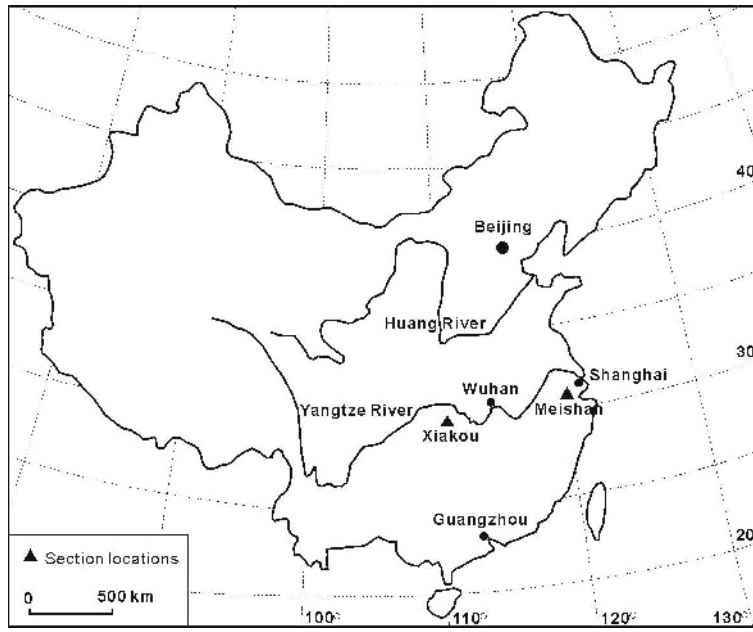

Figure 1. A generalized map showing the locations of the PTB sections.

gray-yellow clay, and bed 29 (18 cm thick) is a gray packstone. At Meishan, the major episode occurred at clay beds 25–26 while the preludial extinction commenced at the packstone bed 24e, which consists of the extinct corals, mostly fusulinids and pseudotirolitid ammonoids, many brachiopods (Yin *et al*., 2007b), a small number of cyanobacteria, a flourish of green sulfur bacteria (Xie *et al*., 2005), and reduced-size conodonts (Luo *et al*., 2008). A globally negative carbon isotope excursion was observed at bed 24 and was considered to be caused by environmental changes due to volcanism, while the cause of the event episode was associated with the resulting ecosystem collapse (Xie *et al*., 2007). However, no solid evidence of volcanism at bed 24e was observed; even the relation between the event episodes and their consequences remain enigmatic. Clay mineralogical records could provide evidence of provenance and environmental change of the sediments and are essential in understanding the event episodes of the biotic crisis. However, clay mineralogical study of the preludial extinction layer and its evolution along the PTB set have rarely been undertaken.

In the structure of dioctahedral 2:1 phyllosilicates, the octahedral sheet contains three symmetrically independent sites (one *trans*- and two *cis*-octahedra), which differ in terms of the arrangement of OH groups and oxygen anions coordinating octahedral cations: in the *trans*-octahedra, the OH groups lay diagonally across the space whereas in the *cis*-octahedra the OH groups form a shared edge. Several studies have suggested that the *cv* smectites, discrete *cv* or interstratified *tv*/*cv* illites, or illite fundamental particles in I-S were formed by hydrothermal transformation of volcanic ash or tuff of rhyolitic composition (Cuadros and Altaner, 1998; McCarty and Reynolds, 1995, 2001; Ylagan *et al*., 2000), whereas I-S formed primarily from weathered illitic material typically consisting of *tv* 2:1 layers independent of the number of I and S layers (Drits *et al*., 1997). In the present study, the clay mineralogies of the PTB sediments from the Meishan and Xiakou sections were compared, using XRD and DSC, in order to better understand the volcanism and environment changes associated with the P/T biotic crisis.

SAMPLING AND METHODS

Meishan was situated in an intra-platform depression between an uplift and a platform in the eastern margin of the Palaeo-Tethys Ocean during the P/T transition, and the sediments exhibited transitional aspects of a carbonate ramp from platform to shallow-water sedimentary facies (Yin *et al*., 2001), while the recently found Xiakou PTB section, Xingshan County, Hubei Province, southern China, formed in an open continental-shelf sedimentary environment and has a thicker PTB stratigraphic set (Wang and Xia, 2004; Hong *et al*., 2008). Comparison between different PTB sections from the Tethyan region has commonly been done using conodont biostratigraphy (Tong and Yang, 1999; Korte *et al*., 2004; Xie *et al*., 2007). Conodonts are tooth-like microfossils, with the fragments representing the hard parts of extinct marine creatures' bodies, with apatite skeletons. Conodont zones of the PTB stratigraphic set are usually used as an indicator of age.

https://doi.org/10.1346/CCMN.2011.0590505 Published online by Cambridge University Press

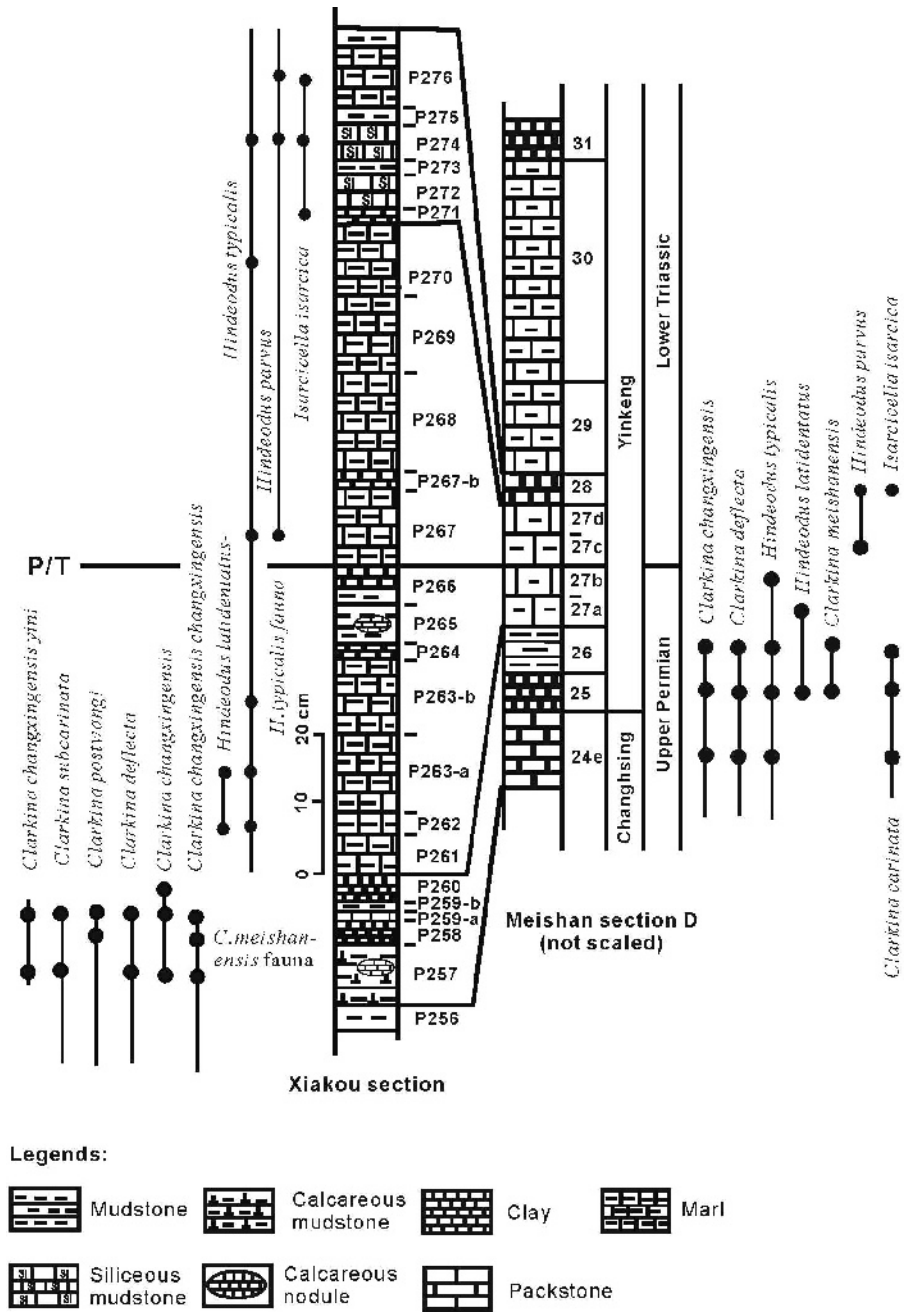

Figure 2. Conodont correlation between the Meishan and the Xiakou PTB stratigraphic sets.

Samples were collected from beds 24d to 29 of the Meishan section, in which all the most severe mass extinction beds of the biotic crisis were included, and from bed P257 to bed P259b of the Xiakou section, in which the preludial extinction bed was included (Figure 2). In the Xiakou section, bed P257 (9.5 cm thick) is a dark gray calcareous mudstone and the overlying bed P258 (3.5 cm thick) is a light gray clay. Bed P259a (2.5 cm thick) is a dolomitic marl and bed P259b (1.5 cm thick) is black clay.

For XRD analysis, bulk samples were air dried and then crushed and ground manually to a grain size of <76 μm using an agate mortar and pestle. Samples of calcareous mudstone and the packstone layers were treated with 0.1 N HCl solution in order to remove carbonates from the detrital materials in the crushed rock. Clay fractions (<2 μm) were separated using the sedimentation method as described by Jackson (1978). The oriented clay-mineral samples were prepared by carefully pipetting the clay suspension onto a glass slide.

https://doi.org/10.1346/CCMN.2011.0590505 Published online by Cambridge University Press

Ethylene glycol-saturated samples were prepared by treating the oriented samples in a container with ethylene glycol at 70ºC for 3 h. The XRD analysis was performed using a Rigaku D/Max-IIIa diffractometer (Rigaku Corporation, Tokyo, Japan) with Ni-filtered CuKα radiation from 3 to 65º2θ at a scan rate of 4º2θ/min, at 35 kV and 35 mA and with 1º divergence, 1º anti-scatter, and 0.3 mm receiving slits.

The clay minerals illite, chlorite, and illite-smectite were identified using characteristic reflections at 10.0, 14.2, and ~11 Å, respectively, while kaolinite was determined by the 002 reflection at 3.57 Å. Mixed-layer I-S clays of the samples had basal 001 spacings of ~11 Å, displaying a relatively broad 001 peak. Semi-quantitative estimation of clay-mineral proportions was undertaken using the weighting factor method (Weir *et al*., 1975; Islam and Lotse, 1986; Bronger *et al*., 1998). Semi-quantitative analysis of clay phases was performed in the air-dried sample for the ~11 Å peak separates with two reflections, with varied intensity ratios among the samples due to their different illite and smectite layer contents in the I-S, after glycolation. The weighting factors of the above-mentioned characteristic peaks of clay minerals were measured prior to quantification analysis, as suggested by Kahle *et al*. (2002). The pure mixed-layer I-S of P259a was used as the standard mixed-layer I-S in the measurements. The results showed that weighting factors of I-S, illite, kaolinite, and chlorite were 7.5, 5.0, 1, and 1.3, respectively, in reasonable agreement with those proposed by Schwertmann and Niederbudde (1993). The detection limits were 1% for kaolinite and chlorite, 3% for illite, and ~5% for mixed-layer I-S.

The proportion of illite in I-S clays is usually estimated using the characteristic peaks near 17º2θ and 9º2θ (CuKα) in the XRD patterns of glycolated clays (Moore and Reynolds, 1997). Such peaks are often overlapped with reflections of other clay species, however, making accurate measurement of the peak positions difficult. Some of the samples from the PTB stratigraphic sets contain only minor amounts of I-S; in the present study, the percentage of illite layers in I-S was determined using the 001 position method (Lu *et al*., 1993), which has the advantage of working on a peak always present at high intensity and free of peak interferences. The composition of the I-S was calculated using the following equation: $1/d_{001}(\text{I-S}) = \alpha/d_{001}(\text{I}) + \beta/d_{001}(\text{S})$, where α was the illite layer content and β was the smectite layer content in the mixed-layer I-S, with the relationship $\alpha + \beta = 1$; d_{001}(I-S) was the 001 reflection of the mixed-layer I-S, d_{001}(I) and d_{001}(S) were the 001 reflections of illite and smectite, with *d* values of 10 Å and 15.5 Å, respectively.

The dehydroxylation of *tv* clay minerals proceeded in a single stage, when each set of two adjacent OH groups was replaced by a single residual oxygen atom. In this case, dehydroxylation occurred at temperatures of <600ºC for illite and smectite layers alike. Dehydroxylation of *cv* structures occurred in two stages, however. At first, each of the two adjacent hydroxyls was replaced by a residual oxygen atom, and the cations that originally occupied *cis*- and *trans*-sites became 5- and 6-coordinated, respectively. With further heating, each cation initially occupying a *trans*-site migrated to the nearest five-fold coordination polyhedron corresponding to the initially vacant *cis*-site, and the resulting structure was the same as that in the case of dehydroxylated *tv* layers. The rearrangement of *cv* structure required additional thermal energy and the dehydroxylation temperature increased to >650ºC (Drits *et al*., 1995). For interstratified *tv*/*cv* clay minerals, dehydroxylation of structural water above and below 600ºC were proportional to the numbers of *cv* and *tv* layers (Drits *et al*., 1998; Drits, 2003). A dehydroxylation temperature of >650ºC indicated that the clay minerals consist of *cv* layers and had a volcanic origin, whereas a dehydroxylation temperature below ~600ºC suggested that the clay minerals consist of mainly *tv* layers and had a terrigenous origin (Deconinck and Chamley, 1995; Drits *et al*., 1995, 1998; Lindgreen and Surlyk, 2000).

The DSC analysis of clay minerals was undertaken using a NETZSCH STA-409 thermal analyzer (NETZSCH Group, Selb, Germany) that can perform DSC and thermogravimetric analyses simultaneously. Approximately 10 mg of the ground samples was added to a corundum crucible for DSC analysis and heated in air from an ambient temperature to 900ºC at a rate of 10ºC min^{-1}. The endothermic and exothermic effects were recorded on a differential curve and were used qualitatively to determine the dehydroxylation temperature of the two types of vacant octahedral sheets in I-S and illite.

RESULTS

Clay-mineral composition of beds

The XRD patterns and clay-mineral proportions of the samples (Figure 3 and Table 1) revealed that the clay minerals of packstone bed 24d contain 91% illite and 9% kaolinite. Bed 24e contains ~20% insoluble detrital materials of mainly quartz, feldspars, and clay minerals, the latter consisting of 56% I-S, 39% illite, and 5% kaolinite. Clay minerals of clay bed 25 are 95% I-S and 5% kaolinite, and the dark gray clay bed 26 consists of 67% illite, 26% I-S, 4% kaolinite, and 3% chlorite. The marl beds 27a to 27d have similar clay mineral compositions of ~90% illite and ~10% kaolinite. Analogous to bed 25, clay bed 28 contains 98% I-S and 2% kaolinite. Clay minerals of the packstone bed 29 are 85% illite, 11% kaolinite, and 4% chlorite. The relative proportions of each clay mineral vary remarkably in different layers along the Meishan section (Figure 4).

https://doi.org/10.1346/CCMN.2011.0590505 Published online by Cambridge University Press

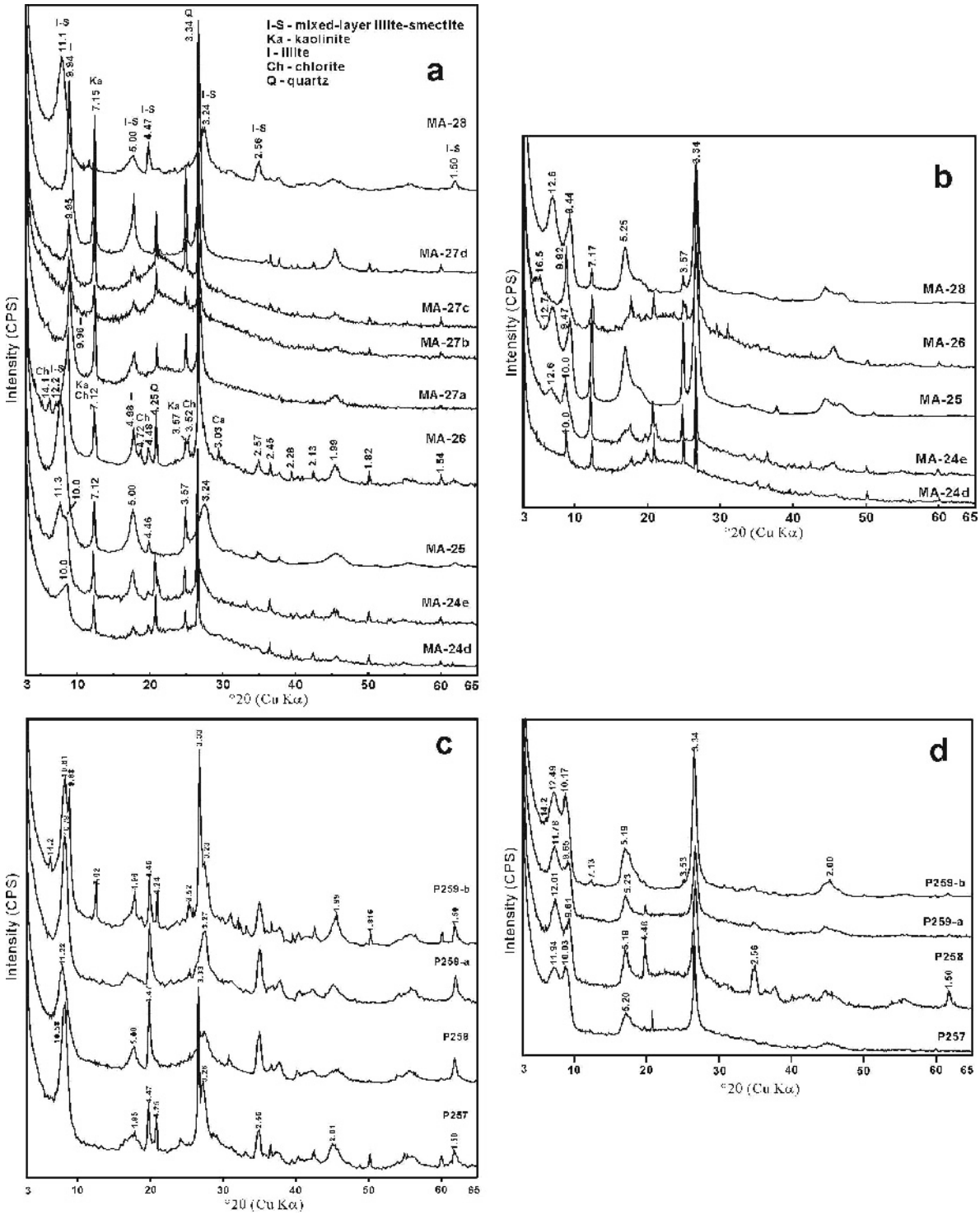

Figure 3. XRD patterns of clay fractions: (a) air-dried clays from the Meishan section; (b) glycolated samples selected from the lithological layers of the Meishan section; (c, d) air-dried and glycolated clays, respectively, from the Xiakou section.

https://doi.org/10.1346/CCMN.2011.0590505 Published online by Cambridge University Press

Table 1. Clay mineral components of clay fractions of the PTB sediments (vol.%).

Location	Bed	I-S	Illite	Kaolinite	Chlorite	S content in I-S (%)
Meishan	24d	–	91	9	–	–
	24e	56	39	5	–	32
	25	95	–	5	–	40
	26	26	67	4	3	50
	27a	–	92	8	–	–
	27b	–	89	11	–	–
	27c	–	88	12	–	–
	27d	–	90	10	–	–
	28	98	–	2	–	27
	29	–	85	11	4	–
Xiakou	P257	100	–	–	–	15
	P258	100	–	–	–	31
	P259a	100	–	–	–	20
	P259b	70	20	–	10	16

In the Xiakou section, the dark gray calcareous mudstone bed P257, the light gray clay bed P258, and the dolomitic marl bed P259a contain only pure I-S clays, while the black clay bed P259b consists of 70% I-S, 20% illite, and 10% chlorite (Table 1).

The 001 reflection of I-S clays displays a relatively broad peak at ~11 Å in the air-dried samples, and it is separated into two peaks at ~12 and ~9.5 Å, respectively, after ethylene glycol salvation (Figure 3), indicating that the I-S clays had ordered I-S-I mixed-layer structures (Lu *et al*., 1991), taking into account the high intensity and symmetric peak shape of the 001 reflections of the I-S clays. The d_{001} spacing of I-S clay of bed 26 at Meishan expanded to 16.5 Å on glycolation, indicating that it was an irregular mixed-layer illite-smectite.

The numbers of smectite layers in the I-S clays of the Meishan and Xiakou sediments were calculated from the XRD profiles. The results (Table 1) showed that I-S clays of beds 24e, 25, 26, and 28 in the Meishan section contain 32, 40, 50, and 27% smectite layers, respectively, while those of beds P257, P258, P259a, and P259b at the Xiakou section contain 15, 31, 20, and 16% smectite layers, respectively.

DSC data

The DSC patterns of clay fractions of the P/T sediments exhibited an endothermic reaction between 500 and 700ºC resulting from the dehydroxylation of the clays (Figure 5). The endothermic peaks of beds 24d and 26 of the Meishan section are wide and flat, having

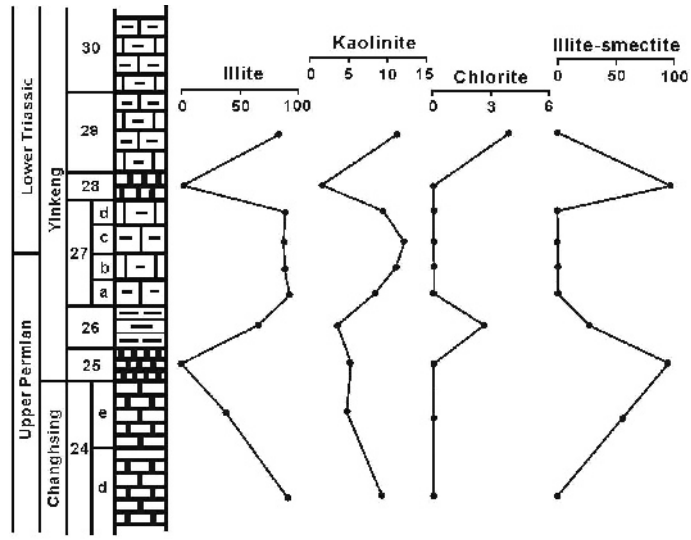

Figure 4. Proportions of clay minerals in the Meishan PTB sediments.

https://doi.org/10.1346/CCMN.2011.0590505 Published online by Cambridge University Press

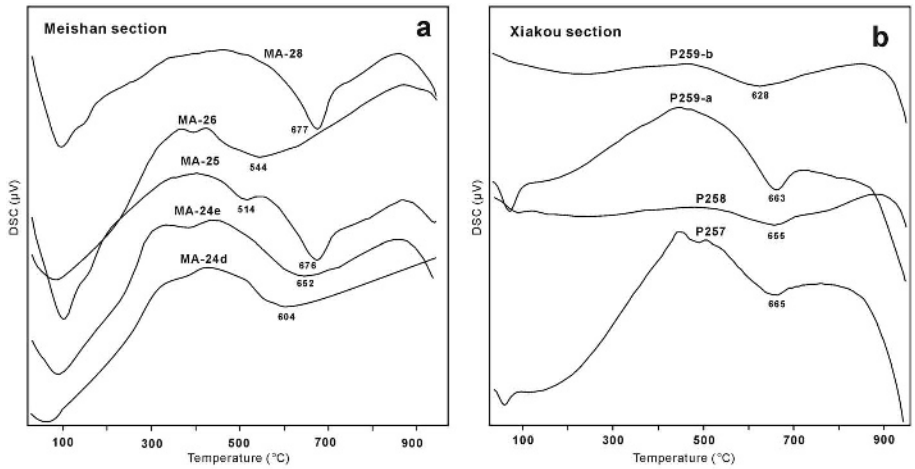

Figure 5. DSC curves of the samples showing dehydroxylation temperatures of: (a) the Meishan section; and (b) the Xiakou section.

dehydroxylation temperatures of 604 and 544ºC, respectively, while those of beds 24e, 25, and 28 exhibit sharp endothermic peaks, having dehydroxylation temperatures of 652, 676, and 677ºC, respectively (Figure 5a). Like the dehydroxylation of clay minerals of the Meishan sediments, beds P257, P258, and P259a of the Xiakou section also showed strong endotherms at 665, 655, and 663ºC, respectively, while that of bed P259b had a weak and wide endotherm at 628ºC (Figure 5b).

DISCUSSION

Origin of clay minerals in beds of the P/T sections

Variations in the number and type of discrete clay minerals in the sediments can be attributed to different parent rocks, changes in weathering conditions in the source area, pedogenesis, clay-mineral segregation during transport and deposition, or diagenesis (Chamley, 1989). Kaolinite formed as a result of intense chemical weathering on land under possibly tropical conditions where abundant rainfall favored ionic transfer and pedogenic development (Millot, 1970; Hallam *et al*., 1991). Although authigenic kaolinite could also have been formed in early diagenesis by circulation of meteoritic water, which may have removed alkali elements in solution and resulted in the formation of kaolinite, it is often formed in sandstones with high porosity (Dera *et al*., 2009). The PTB stratigraphic set at Meishan consisted mainly of marl and packstone of low porosity so diagenetic processes could not be responsible for the occurrence of kaolinite in the PTB sediments.

Illite in marine sediments is generally considered to be of continental origin (Biscay, 1965; Singer, 1984; Weaver, 1989; Robert and Kennett, 1994). Burial diagenesis could also cause the transformation of kaolinite into illite and/or chlorite. However, beds 26 and 28 have the smallest kaolinite content while beds 24d, 27c, and 29 have the largest kaolinite content (Figure 4); the sharp changes in kaolinite content along the PTB section at Meishan suggest no evidence of progressive change with depth, and burial diagenesis was never strong enough to transform the initial kaolinite into illite and/or chlorite. In general, kaolinite displayed strong resistance to illitization under moderate diagenetic conditions (Lanson *et al*., 2002). Chlorite is a stable detrital product of high-latitude climate conditions, where mechanical weathering prevailed, and the assemblage of chlorite and illite is indicative of a weathering origin (Singer, 1984). The presence of illite and kaolinite in marl beds 27a to 27d is, therefore, indicative of a terrigenous provenance.

Smectite usually forms as a result of intense chemical weathering in poorly drained, tropical to subtropical areas of low relief, marked by flooding during humid seasons and substantial pore water in the soil during dry seasons (Chamley, 1989). In marine sediments, however, smectite is considered to be the predominant authigenic clay mineral (Clauer *et al*., 1990), and the interbedded pure smectite beds in marine sediments are usually derived from marine alteration of volcanic ashes (Pellenard *et al*., 2003). Smectites and illites generally consist of *cis*-vacant (*cv*) and *trans*-vacant (*tv*) 2:1 layers, respectively (Tsipurski and Drits, 1984; Drits and Zviagina, 2009). Formation of 2:1 illite layers from smectite layers in I-S clays should result in an increase in the number the *cv* 2:1 layers, suggesting that structures of I-S with dominant *cv* 2:1 layers were, therefore, derived from altered volcanic materials, while those with mainly *tv* 2:1 layers were derived from weathered illite (Altaner and Ylagan, 1997; Cuadros and Altaner, 1998; Drits *et al*., 1998; Lindgreen and Surlyk, 2000; McCarty and Reynolds, 1995, 2001).

The I-S clays are only present in certain layers of the PTB stratigraphic sets according to the XRD analysis. The major mineral I-S could represent a major smectitic volcanogenic component that was converted to I-S by alteration (Pearson, 1990; Cuadros and Altaner, 1998; McCarty and Reynolds, 2001; Pellenard *et al*., 2003;

https://doi.org/10.1346/CCMN.2011.0590505 Published online by Cambridge University Press

Meunier *et al*., 2004), or it could be a terrigenous weathering product, formed in a weathering environment through the leaching and degradation of a precursor illite and under climates with alternating dry/wet seasons (Chamley, 1989; Vanderaveroet and Deconinck, 1997; Hong *et al*., 2007; Hong *et al*., 2010). In addition, mixed-layer I-S clay could also be formed by smectite illitization during diagenesis, which often took place at the temperature of oil formation (Reynolds and Hower, 1970). The P-T sediments in southern China were mature enough for oil generation (Wang, 1998), and so illitization of smectite with increases in illite-layer content and in the order of the layer-type distribution in the I-S clays would be expected. As shown by the XRD analysis, the I-S clays at Meishan contained 50–73% illite layers while those at Xiakou have 69–85% illite layers. The high proportion of illite layers in I-S clays suggests that the illite components may result from the illitization of volcanogenic smectite during diagenesis (Hower *et al*., 1976; Pearson and Small, 1988). In the Meishan section clay bed 28, however, having I-S with 73% illite layers is situated in the upper part while bed 26 having I-S with 50% illite layers is situated in the lower part of the section. In the Xiakou section, bed P258 having I-S with 69% illite layers was interbedded with bed P257 having I-S with 85% illite layers and bed P259a having I-S with 80% illite layers. Within such a small thickness of sediments (~40 cm at Meishan and ~20 cm at Xiakou), differences in burial temperatures were not responsible for the formation of I-S with different amounts of illite layers. Variations in the numbers of illite layers in the I-S clays of the PTB sediments can thus be attributed to different parent materials, *i.e*. different chemical compositions of the ashes in different ash beds.

Determination of *tv* and *cv* layers in illites and I-S was examined by XRD of randomly oriented powders. The broader reflections from I-S owing to interstratification and rotational disorder precluded the precise location of peak positions, however, and made the precise determination of *tv* and *cv* layers in I-S difficult. Where the I-S exhibited a turbostratic structure, in particular, and where the XRD pattern contained only basal reflections and two-dimensional *hk* diffraction bands, *tv* and *cv* layers in illites and I-S could not be determined using the XRD method (Drits *et al*., 2002). However, the *tv* and *cv* octahedral sheets of the 2:1 clays have different dehydroxylation temperatures. This difference is, therefore, commonly used to determine the *tv* and *cv* layers in clay minerals (Deconinck and Chamley, 1995; Drits *et al*., 1998; Lindgreen and Surlyk, 2000; Hong *et al*., 2008).

Clay minerals of bed 25 consist of 95% I-S and 5% kaolinite. Dehydroxylation of kaolinite usually took place at a temperature between 500 and 560ºC, coincident with that of the *tv* layers in I-S and illite. The endothermic effect from kaolinite can be estimated roughly from the relative proportion of kaolinite according to the XRD analysis. As shown in Figure 5, on the DSC curve of bed 25, the endothermic effect at 514ºC could be attributed to dehydroxylation of kaolinite while that at 676ºC could be attributed to dehydroxylation of the *cv* layers in the I-S clays, respectively. Bed 28 contains 98% I-S and 2% kaolinite; only one strong endotherm at 677ºC was observed, suggesting that the I-S clays of bed 28 were derived from a volcanic smectite precursor which originated from submarine alteration of volcanic ash, in good agreement with the identification of primary volcanic crystals such as zircon, β-quartz, and apatite in these clay beds (Yin *et al*., 1992).

In view of the impact event, the event horizon was produced by a mixture of terrestrial ejecta and meteoritic material, or a mixture of ash, terrestrial ejecta, and meteoritic material. The contents of the beds should be relatively homogeneous and mineralogically similar at the two localities because of mixing during the impact process (Smit and Klaver, 1981). Comparing the Meishan and the Xiakou sections, the clay mineralogy of the two clay beds 25 at Meishan and P258 at Xiakou (correlated using conodonts) was different. Bed P258 consists of I-S only, while bed 25 contains I-S and kaolinite. Kaolinite is one of the most common soil-derived clay minerals. The P-T sediments consist of mainly marl and packstone with low porosity, excluding the genesis of authigenic kaolinite formed during the diagenetic process (Dera *et al*., 2009). On the contrary, kaolinite did not transform to I-S during the burial diagenesis (Lanson *et al*., 2002). Different clay compositions of the event bed between the two P-T sections, therefore, indicated different sedimentary environments for the two locations, *i.e*. influx was the only source of volcanic material in the Xiakou region, while volcanic material in association with weathering of kaolinite was the source in the Meishan area. The clay mineralogy at the two distant sites suggests that clay minerals near the PTB depended on the local sedimentary environment, and argues against a mixture of terrestrial ejecta and meteoritic material, or a mixture of ash, terrestrial ejecta, and meteoritic material simultaneously in different locations.

Clay minerals of bed 24d, having 91% illite and 9% kaolinite, dehydroxylated at 604ºC, and those of bed 26, having 67% illite, 26% I-S, 4% kaolinite, and 3% chlorite, dehydroxylated at 544ºC (Figure 5). The dehydroxylation behavior of bed 24d is mainly attributed to illite, *i.e.* the wide and flat peak of illite dehydroxylation at ~600ºC, suggesting that illite in the sediments originated from continental weathering (Deconinck and Chamley, 1995). Again, the dehydroxylation of bed 26 is mainly attributed to illite and I-S, and the dehydroxylation temperature at 544ºC also indicates that illite and I-S of bed 26 originated from continental weathering. Clay minerals of bed 24e consist of 56% I-S, 39% illite,

https://doi.org/10.1346/CCMN.2011.0590505 Published online by Cambridge University Press

and 5% kaolinite, and the dehydroxylation temperature was 652ºC, indicating that the I-S and illite in bed 24e had a volcanic origin. Beds P257, P258, and P259a at the Xiakou section contain only I-S clays, while bed P259b contains 70% I-S, 20% illite, and 10% chlorite. Dehydroxylation temperatures of I-S clays of beds P257, P258, and P259a were 665, 655, and 663ºC, respectively, suggesting that clay minerals in these beds originated from submarine alteration of volcanic ashes. In contrast, the endotherm at 628ºC of illite and I-S of bed P259b was indicative of a mixture of terrigenous provenance and diagenetic alteration of volcanic ashes in marine sediments (Hong *et al*., 2008).

Volcanism and environment change across the PTB

In southern China, the PTB stratigraphic set at different locations contained different ash layers, *e.g.* four volcanic ash layers were present at Meishan while eight were present at Xiakou; most of the ash beds show no evidence of mass extinction. The severe extinction horizons at Meishan were recorded in the packstone bed 24e (the prelude of the main episode), beds 25 and 26 (the event beds), and bed 28 (the second episode), respectively (Yin *et al*., 2007a, 2007b). In comparison with the ash layer, the occurrence of volcaniclastic-derived clays in the packstone bed 24e indicate an ash influx by distal transport during the episode. At Xiakou, one of the mass extinction horizons was also observed in the calcareous mudstone bed P257, with conodont correlation to the packstone bed 24e at Meishan (Figure 2). Analogous to bed 24e at Meishan, the calcareous mudstone bed P257 contains only I-S clay of volcanic origin, indicating more ash influx at Xiakou than at Meishan; such wide-spread volcanic ash and synchronous sedimentation with carbonate in the sediments suggests that medium-acidic volcanism took place along Panthalassa during the episode and the Xiakou area was closer to the volcanic source than the Meishan region (Yin *et al*., 1992; Veevers and Tewari, 1995; Yin *et al*., 2007a).

Sulfur isotope records of the Meishan sediments have been investigated intensively and all the results exhibit a similar trend with positive shifts of the $^{34}S/^{32}S$ ratio of carbonate-associated sulfate in bed 24e. In recent studies, the highest concentration of ^{34}S and the largest ion ratio ($^{34}S/^{32}S$) for sulfide has also been reported in bed 24e (Kaiho *et al*., 2006; Jiang *et al*., 2006) and was considered to be of volcanic origin as the $^{34}S/^{32}S$ value of 2.2‰ is coincident with that of a volcanic source for the sulfur (Jiang *et al*., 2006). High concentrations of sulfide at and just below the terrestrial PTB were also observed in the northern Karoo basin, South Africa, and a volcanic origin of sulfur was suggested (Maruoka *et al*., 2003). High concentrations of sulfide with volcanic sulfur source at distant sites lead to the suggestion that massive release of volcanic H_2S took place during the period, and sulfide toxicity was suggested as the driving force of the mass extinction (Grice *et al*., 2005; Payne and Kump, 2007). Volcanic materials in bed 24e coincident with the prelude of the main episode of mass extinction reinforced the temporal link between volcanism and the mass extinction.

The black clay bed 26, one of the severe mass-extinction horizons, is isochronous with layer P259b in the Xiakou section, according to conodont correlation between the two PTB sets (Wang and Xia, 2004). Both the black clay bed 26 in Meishan and P259b in Xiakou show the same features of black color, condensed texture, and lamination. However, P259b contains 70% I-S, 20% illite, and 10% chlorite, which were derived from a mixture of terrigenous and volcanic sources (Hong *et al*., 2008), while bed 26 consists of 67% illite, 26% I-S, and minor kaolinite and chlorite, having a terrigenous origin (Table 1). The difference in clay mineralogy between bed 26 at Meishan and bed P259b at Xiakou probably resulted from their different sedimentary environments; Meishan was situated closer to the volcanic eruption than Xiakou (Wang and Xia, 2004). Kaolinite deposits typically occur near the shore because of the large particles; the occurrence of kaolinite at Meishan while absent from Xiakou could be attributed to differential settling of clay minerals during the sedimentary process, and volcanic I-S in P259b at Xiakou could be attributed to illitization of the volcanic smectite precursor. In addition, the XRD results show a significant increase in quartz and feldspar abundance in these black clay layers. This increased detrital influx also suggested stronger physical weathering.

Chlorite is a common mineral of greenschist-facies metamorphic rocks, also found in sedimentary rocks; it can survive repeated cycles of erosion. Chlorite typically exists in cold/arid areas of very low rates of chemical weathering and areas of steep relief where mechanical erosion interferes with soil formation (Chamley, 1989; Weaver, 1989). Intense chemical weathering can cause the transformation of chlorite to kaolinite during the weathering process. The occurrence of chlorite and illite in the black beds in both the Meishan and Xiakou sections may, therefore, reflect the increased erosion of soils and poorly chemically weathered parent rocks, which could result from higher relief due to regression. Previous studies have indicated, however, that during the period in question the much stronger regression took place at bed 24 rather than at bed 26 (Hallam and Wignall, 1999). In bed 24, where the most intense regression occurred, no chlorite was observed in the period when increased mechanical erosion was expected for the regression-derived higher relief. Hence, the presence of chlorite in the episode of mass extinction of bed 26 in Meishan and P259b in Xiakou could be indicative of a rapid palaeoenvironmental change from warm/humid to cold/dry climatic conditions. The small kaolinite content in bed 26 in Meishan, counterbalanced by increases in chlorite and illite, is attributed to a

https://doi.org/10.1346/CCMN.2011.0590505 Published online by Cambridge University Press

decrease in chemical weathering and to enhanced mechanical erosion under a cooler, more arid climate, while the notable increase in kaolinite content in bed 27 indicates a climate change from cool/arid to warm/humid conditions, in good agreement with the notably high Mg/Ca values of the Meishan PTB sediments (Yang and Wu, 2006).

CONCLUSIONS

Bed 25 contains 95% I-S and 5% kaolinite, while bed 28 contains 98% I-S and 2% kaolinite. The dehydroxylation behavior of these clays is indicative of a volcanic smectite precursor. Clay minerals of the preludial mass-extinction horizon bed 24e at Meishan include 56% I-S, 39% illite, and 5% kaolinite, with a dehydroxylation temperature of 652ºC, and the conodont-correlated calcareous mudstone bed P257 at Xiakou contains only I-S clay, with a dehydroxylation temperature of 665ºC. These observations suggest that either the I-S and illite in bed 24e at Meishan or the I-S in bed P257 at Xiakou contained mainly *cv* layers and, therefore, were of volcanic origin. Volcanism in association with the preludial mass extinction reinforces the temporal link between volcanism and the mass extinction.

Clay minerals of the black clay bed 26 at Meishan comprise 67% illite, 26% I-S, 4% kaolinite, and 3% chlorite, with dehydroxylation occurring at 544ºC, suggesting that clay minerals of bed 26 have a terrigenous origin. The conodont-correlated black clay bed P259b at Xiakou contains 70% I-S, 20% illite, and 10% chlorite, with a dehydroxylation temperature of 628ºC, indicating that clays of P259b were derived from a mixture of terrigenous and volcanic sources. Different clay mineralogies between bed 26 at Meishan and bed P259b at Xiakou probably resulted from different sedimentary environments; large amounts of I-S, illite, and chlorite in sediments suggest a period of rapid erosion and cold/dry climate conditions.

ACKNOWLEDGMENTS

The present work was supported by the Natural Science Foundation of China (allotment grant numbers 41072030 and 40872038). The authors thank Dr M.Z. He for the DSC analysis, Dr J.S. Yu for the XRD analysis, Prof. Timothy Kusky for improving the English, and Prof. J.W. Stucki, Editor in Chief, Prof. H.L. Dong, Associate Editor, and Prof. F. Nieto and the two anonymous reviewers for their insightful reviews, valuable comments, and suggestions.

REFERENCES

Altaner, S.P. and Ylagan, R.F. (1997) Comparison of structural models of mixed-layer illite-smectite and reaction mechanisms of smectite illitization. *Clays and Clay Minerals*, **45**, 517–533.

Basu, A.R., Petaev, M.I., Poreda, R.J., Jacobsen, S.B., and Becker, L. (2003) Chondritic meteorite fragments associated with the Permian-Triassic boundary in Antarctica. *Science*, **302**, 1388–1392.

Becker, L., Poreda, R.J., Hunt, A.G., Bunch, T.E., and Rampino, M. (2001) Impact event at the Permian-Triassic boundary: Evidence from extraterrestrial noble gases in fullerenes. *Science*, **291**, 1530–1533.

Biscaye, P.E. (1965) Mineralogy and sedimentation of recent deep-sea clay in the Atlantic Ocean and adjacent seas and oceans. *Geological Society of America Bulletin*, **76**, 803–832.

Bronger, A., Winter, R., and Sedov, S. (1998) Weathering and clay mineral formation in two Holocene soils and in buried paleosols in Tadjikistan: towards a Quaternary paleoclimatic record in Central Asia. *Catena*, **34**, 19–34.

Chamley, H. (1989) *Clay Sedimentology*. Springer Verlag, Berlin, 623 pp.

Clauer, N., O'Neil, J.R., Bonnot-Courtois, C., and Holtzapffel, T. (1990) Morphological, chemical, and isotopic evidence for an early diagenetic evolution of detrital smectite in marine sediments. *Clays and Clay Minerals*, **38**, 33–46.

Courtillot, V. and Olson, P. (2007) Mantle plumes link magnetic superchrons to Phanerozoic mass depletion events. *Earth and Planetary Science Letters*, **260**, 495–504.

Cuadros, J. and Altaner, S.P. (1998) Characterization of mixed-layer illite-smectite from bentonites using microscopic, chemical, and X-ray methods: Constraints on the smectite-to-illite transformation mechanism. *American Mineralogist*, **83**,762–774.

de Wit, M.J., Ghosh, J.G., de Villiers, S., Rakotosolofo, N., Alexander, J., Tripathi, A., and Looy, C. (2002) Multiple organic carbon isotope reversals across the Permo-Triassic boundary of terrestrial Gondwana sequences: clues to extinction patterns and delayed ecosystem recovery. *Journal of Geology*, **110**, 227–246.

Deconinck, J.F. and Chamley, H. (1995) Diversity of smectite origins in late Cretaceous sediments: Example of chalks from northern France. *Clay Minerals*, **30**, 365–379.

Dera, G., Pellenard, P., Neige, P., Deconinck, J.F., Pucéat, E., and Dommergues J.L. (2009) Distribution of clay minerals in Early Jurassic Peritethyan seas: Palaeoclimatic significance inferred from multiproxy comparisons. *Palaeogeography, Palaeoclimatology, Palaeoecology*, **271**, 39–51.

Drits, V.A. (2003) Structural and chemical heterogeneity of layer silicates and clay minerals. *Clay Minerals*, **38**, 403–432.

Drits, V.A. and Zviagina, B.B. (2009) *Trans*-vacant and *cis*-vacant 2:1 layer silicates: Structural features, identification, and occurrence. *Clays and Clay Minerals*, **57**, 405–415.

Drits, V.A., Besson, G., and Muller, E. (1995) An improved model for structural transformation of heat-treated aluminous dioctahedral 2:1 layer silicates. *Clays* and *Clay Minerals*, **43**, 718–731.

Drits, V.A., Sakharov, B.A., Lindgreen, H., and Salyn, A. (1997) Sequential structural transformation of illite-smectite-vermiculite during diagenesis of Upper Jurassic shales from the North Sea and Denmark. *Clay Minerals*, **32**, 351–372.

Drits, V.A., Lindgreen, H., Salyn, A.L., Ylagan, R., and McCarty, D.K. (1998) Semiquantitative determination of *trans*-vacant and *cis*-vacant 2:1 layers in illites and illite-smectites by thermal analysis and X-ray diffraction. *American Mineralogist*, **83**, 1188–1198.

Drits, V.A., Sakharov, B.A., Dainyak, L.G., Salyn, A.L., and Lindgreen, H. (2002) Structural and chemical heterogeneity of illite-smectites from Upper Jurassic mudstones of East Greenland related to volcanic and weathered parent rocks. *American Mineralogist*, **87**, 1590–1607.

Erwin, D.H. (1994) The Permo-Triassic extinction. *Nature*, **367**, 231–236.

Grasby, S.E. and Beauchamp, B. (2009) Latest Permian to

Early Triassic basin-to-shelf anoxia in the Sverdrup Basin, Arctic Canada. *Chemical Geology*, **264**, 232–246.

Grice, K., Cao, C., Love, G.D., Böttcher, M.E., Twitchett, R.J., Grosjean, E., Summons, R.E., Turgeon, S.C., Dunning, W., and Jin Y. (2005) Photic zone euxinia during the Permian-Triassic superanoxic event. *Science*, **307**, 706–709.

Hallam, A. and Wignall, P.B. (1997) *Mass Extinctions and their Aftermath*. Oxford, Oxford University Press, 330 pp.

Hallam, A. and Wignall, P.B. (1999) Mass extinctions and sea-level changes. *Earth Science Reviews*, **48**, 217–250.

Hallam, A., Grose, J.A., and Ruffell, A.H. (1991) Paleoclimatic significance of changes in clay mineralogy across the Jurassic-Cretaceous boundary in England and France. *Palaeogeography. Palaeoclimateology, Palaeoecology*, **81**, 173–187.

Heydari, E. and Hassanzadeh, J. (2003) Deev Jahi model of the Permian-Triassic boundary mass extinction: a case for gas hydrates as the main cause of biological crisis on Earth. *Sedimentary Geology*, **163**, 147–163.

Holser, W.T., Schölaub, H.-P., Attrep, M., Boeckelmann, K., Klein, P., Magaritz, M., Orth, C.J., Fenninger, A., Jenny, C., Kralik, M., Mauritsch, H., Pak, E., Schramm, J.-M., Stattegger, K., and Schmöler, R. (1989) A unique geochemical record at the Permian/Triassic boundary. *Nature*, **337**, 39–44.

Hong, H.L., Li, Z., Xue, H.J., Zhu, Y.H., Zhang, K.X., and Xiang, S.Y. (2007) Oligocene clay mineralogy of the linxia basin: Evidence of paleoclimatic evolution subsequent to the initial-stage uplift of the Tibetan plateau. *Clays and Clay Minerals*, **55**, 491–503.

Hong, H.L., Zhang, N., Li, Z.H., Xue, H.J., Xia, W.C., and Yu, N. (2008) Clay mineralogy across the P/T boundary of the Xiakou section, China: evidence of clay provenance and environment. *Clays and Clay Minerals*, **56**, 131–143.

Hong, H.L., Gu, Y.S., Li, R.B., Zhang, K.X., and Li, Z.H. (2010) Clay mineralogy and geochemistry and their palaeoclimatic interpretation of the Pleistocene deposits in the Xuancheng section, southern China. *Journal of Quaternary Science*, **25**, 662–674.

Hower, J., Eslinger, E.V., Hower, M.E., and Perry, E.A. (1976) Mechanism of burial metamorphism of argillaceous sediment: 1. Mineralogical and chemical evidence. *Geological Society of America Bulletin*, **87**, 725–737.

Islam, A.K.M.E. and Lotse, E.G. (1986) Quantitative mineralogical analysis of some Bangladesh soils with X-ray, ion exchange and selective dissolution techniques. *Clay Minerals*, **21**, 31–42.

Jackson, M.L. (1978) *Soil Chemical Analyses*. Authors' publication Univ. of Wisconsin Madison, USA.

Jiang, Y., Tang, Y., Dai, S., Zou, X., Qian, H., and Zhou, G. (2006) Pyrite and sulfur isotopic composition near the Permian-Triassic boundary in Meishan, Zhejiang. *Acta Geologica Sinica*, **80**, 1202–1207 (in Chinese with English abstract).

Jin, Y.G., Wang, Y., Wang, W., Shang, Q.H., Cao, C.Q., and Erwin, D.H. (2000) Pattern of marine mass extinction near the Permian-Triassic boundary in south China. *Science*, **289**, 432–436.

Kahle, M., Kleber, M., and Jahn, R. (2002) Review of XRD-based quantitative analyses of clay minerals in soils: the suitability of mineral intensity factors. *Geoderma*, **109**, 191–205.

Kaiho, K., Kajiwara, Y., Chen, Z.Q., and Gorjan, P. (2006) A sulfur isotope event at the end of the Permian. *Chemical Geology*, **235**, 33–47.

Kidder, D.L. and Worsley, T.R. (2003) Causes and consequences of extreme Permo-Triassic warming to globally equable climate and relation to the Permo-Triassic extinction and recovery. *Palaeogeography, Palaeoclimatology, Palaeoecology*, **203**, 207–237.

Knoll, A.H., Bambach, R.K., Payne, J.L., Pruss, S., and Fischer, W.W. (2007) Paleophysiology and end-Permian mass extinction. *Earth and Planetary Science Letters*, **256**, 295–313.

Korte, C. and Kozur, H.W. (2010) Carbon-isotope stratigraphy across the Permian-Triassic boundary: A review. *Journal of Asian Earth Sciences*, **39**, 215–235.

Korte, C., Kozur, H.W., and Mohtat-Aghai, P. (2004) Dzhulfian to lowermost Triassic delta ^{13}C record at the Permian/Triassic boundary section at Shahreza, Central Iran. *Hallesches Jahrbuch für Geowissenschaften, Reihe B. Beiheft*, **18**, 73–78.

Kump, L.R., Pavlov, A., and Arthur, M.A. (2005) Massive release of hydrogen sulfide to the surface ocean and atmosphere during intervals of oceanic anoxia. *Geology*, **33**, 397–400.

Lanson, B., Beaufort, D., Berger, G., Bauer, A., Cassagnabère, A., and Meunier, A. (2002) Authigenic kaolin and illitic minerals during burial diagenesis of sandstones: A review. *Clay Minerals*, **37**, 1–22.

Lindgreen, H. and Surlyk F. (2000) Upper Permian-Lower Cretaceous clay mineralogy of East Greenland: provenance, palaeoclimate and volcanicity. *Clay Minerals*, **35**, 791–806

Lu, Q., Lei, X.R., and Liu, H.F. (1991) Genetic types and crystal chemical classification of irregular illite/smectite interstratified clay minerals. *Acta Mineralogica Sinica*, **11**, 97–104 (in Chinese with English abstract).

Lu, Q., Lei, X.R., and Liu, H.F. (1993) Study of the stacking sequences of a kind of irregular mixed-layer illite-smectite (I/S) clay mineral. *Acta Geologica Sinica*, **67**, 123–130 (in Chinese with English abstract).

Luo, G.M., Lai, X.L., Shi, G.R., Jiang, H.S., Yin, H.F., Xie, S.C., Tong, J.N., Zhang, K.X., He, W.H., and Wignall, P.B. (2008) Size variation of conodont elements of the Hindeodus-Isarcicella clade during the Permian-Triassic transition in South China and its implication for mass extinction. *Palaeogeography Palaeoclimatology Palaeoecology*, **264**, 176–187.

Maruoka, T., Koeberl, C., Hancox, P.J., and Reimold, W.U. (2003) Sulfur geochemistry across a terrestrial Permian-Triassic boundary section in the Karoo Basin South Africa. *Earth and Planetary Science Letters*, **206**, 101–117.

McCarty, D.K. and Reynolds, R.C., Jr. (1995) Rotationally disordered illite-smectite in Paleozoic K-bentonites. *Clays and Clay Minerals*, **43**, 271–284.

McCarty, D.K. and Reynolds, R.C., Jr. (2001) Three-dimensional crystal structures of illite-smectite minerals in paleozoic K-bentonites from the appalachian basin. *Clays and Clay Minerals*, **49**, 24–35.

Meunier, A., Lanson, B., and Velde, B. (2004) Composition variation of illite-vermiculite-smectite mixed-layer minerals in a bentonite bed from Charente (France). *Clay Minerals*, **39**, 317–332.

Meyer, K.M., Kump, L.R., and Ridgwell, A. (2008) Biogeochemical controls on photiczone euxinia during the end-Permian mass extinction. *Geology*, **36**, 747–750.

Millot, G. (1970) *Geology of Clays*. Springer-Verlag, Berlin, 499 pp.

Moore D.M. and Reynolds, R.C., Jr. (1997) *X-Ray Diffraction and the Identification and Analysis of Clay Minerals*. Oxford University Press, New York, 378 pp.

Payne, J.L. and Kump, L.R. (2007) Evidence for recurrent Early Triassic massive volcanism from quantitative interpretation of carbon isotopic fluctuations. *Earth and Planetary Science Letters*, **256**, 264– 277.

Pearson, M.J. (1990) Clay mineral distribution and provenance in Mesozoic and Tertiary mudrocks of the Moray Firth and northern North Sea. *Clay Minerals*, **25**, 519–541.

Pearson, M.J. and Small, J.S. (1988) Illite-smectite diagenesis and palaeotemperatures in northern North Sea Quaternary to Mesozoic shale sequences. *Clay Minerals*, **23**, 109–132.

Pellenard, P., Deconinck, J.F., Huff, W.D., Thierry, J., Marchand, D., Fortwengler, D., and Trouiller, A. (2003) Characterization and correlation of Upper Jurassic (Oxfordian) bentonite deposits in the Paris Basin and the Subalpine Basin, France. *Sedimentology*, **50**, 1035–1060.

Renne, P.R., Zichao, Z., Richards, M.A., Black, M.T., and Basu, A.R. (1995) Synchrony and causal relations between Permian-Triassic boundary crises and Siberian flood volcanism. *Science*, **269**, 1413–1416.

Retallack, G.J. (2001) A 300-million-year record of atmospheric carbon dioxide from fossil plant cuticles. *Nature*, **411**, 287–290.

Reynolds, R.C. and Hower, J. (1970) The nature of interlayering in mixed-layer illite-montmorillonite. *Clays and Clay Minerals*, **18**, 25–36.

Robert, C. and Kennett, J.P. (1994) Antarctic subtropical humid episode at the Paleocene-Eocene boundary: Clay-mineral evidence. *Geology*, **22**, 211–214.

Schwertmann, U. and Niederbudde, E.A. (1993) *Tonminerale in Böden*. Pp. 212–265 in: *Tonminerale und Tone, Struktur, Eigenschaften, Anwendung und Einsatz in Industrie und Umwelt* (K. Jasmund and G. Lagaly, editors). Steinkopff Verlag, Darmstadt, Germany.

Sheldon, N.D. (2006) Abrupt chemical weathering increase across the Permian-Triassic boundary. *Palaeogeography Palaeoclimatology Palaeoecology*, **231**, 315–321.

Singer, A. (1984) The palaeoclimatic interpretation of clay minerals in sediments. *Earth Science Reviews*, **21**, 251–293.

Smit, J. and Klaver, G. (1981) Sanidine spherules at the Cretaceous-Tertiary boundary indicate a large impact event. *Nature*, **292**, 47–49.

Tong, J.N. and Yang, Y. (1999) Significant progresses on the Lower Triassic conodonts, Meishan, Changxing, Zhejiang province. *Chinese Science Bulletin*, **42**, 2571–2573.

Tsipurski, S.I. and Drits, V.A. (1984) The distribution of octahedral cations in the 2:1 layers of dioctahedral smectites studied by oblique-texture electron diffraction. *Clay Minerals*, **19**, 177–193.

Vanderaveroet, P. and Deconinck, J.F. (1997) *Clay mineralogy of Cenozoic sediments of the Atlantic City Borehole, New Jersey*. Pp. 49–57 in: (K.G. Miller and S.W. Snyder, editors). Proceedings of the ODP, Scientific Results, 150X. Ocean Drilling Program, College Station, Texas, USA.

Veevers, J.J. and Tewari, R.C. (1995) Permian-Carboniferous and Permian-Triassic magmatism in the rift zone bordering the Tethyan margin of southern Pangea. *Geology*, **23**, 467–470.

Wang, G.Q. and Xia, W.C. (2004) Conodont zonation across the Permian-Triassic boundary at the Xiakou section, Yichang city, Hubei province and its correlation with the Global Stratotype Section and Point of the PTB. *Canadian Journal of Earth Sciences*, **41**, 323–330.

Wang, Z.Y. (1998) Permian sedimentary facies and sequence stratigraphy in Daxiakou section, Xingshan county, Hubei province. *Journal of Jianhan Petroleum Institute*, **20**, 1–7 (in Chinese with English abstract).

Weaver, C.E. (1989) *Clays, Muds, and Shales*. Developments in Sedimentology, **44**, Elsevier, Amsterdam, 819 pp.

Wignall, P.B., Morante, R., and Newton, R. (1998) The Permo-Triassic transition in Spitsbergen: $\delta^{13}C_{org}$ chemostratigraphy, Fe and S geochemistry, facies, fauna and trace fossils. *Geological Magazine*, **135**, 47–62.

Wignall, P.B. (2001) Large igneous provinces and mass extinctions. *Earth-Science Reviews*, **53**, 1–33.

Weir, A.H., Ormerod, E.C., and El Mansey, I.M.I. (1975) Clay mineralogy of sediments of the Western Nile Delta. *Clay Minerals*, **10**, 369–386.

Xie, S.C., Pancost, R.D., Yin, H.F., Wang, H.M., and Evershed, R.P. (2005) Two episodes of microbial change coupled with Permo/Triassic faunal mass extinction. *Nature*, **434**, 494–497.

Xie, S.C., Pancost, R.D., Huang, J.H., Wignall, P.B., Yu, J.X., Tang, X.Y., Chen, L., Huang, X.Y., and Lai, X.L. (2007) Changes in the global carbon cycle occurred as two episodes during the Permian-Triassic crisis. *Geology*, **35**, 1083–1086.

Yang, J.X. and Wu, M. (2006) Synchronized oscillations in Phanerozoic chemical composition of seawater, carbonate sedimentation and biotic evolution: Progresses and prospects. *Geological Science and Technology Information*, **25**, 1–7 (in Chinese with English abstract).

Yin, H.F., Huang, S.J., Zhang, K.X., Hansen, H.J., Yang, F.Q., Ding, M.H., and Bie, X.M. (1992) The effects of volcanism on the Permo-Triassic mass extinction in South China. Pp. 169–174 in: *Permo-Triassic Events in the Eastern Tethys* (W.C. Sweet, Z.Y. Yang, J.M. Dickins, and H.F. Yin, editors). Cambridge University Press, Cambridge, UK.

Yin, H.F., Zhang, K.X., Tong, J.N., Yang, Z.Y., and Wu, S.B. (2001) The global stratotype section and point (GSSP) of the Permian-Triassic boundary. *Episodes*, **24**, 102–113.

Yin, H.F., Feng, K.L., Lai, X.L., Baud, A., and Tong, J.N. (2007a) The protracted Permo-Triassic crisis and the multi-act mass extinction around the Permian-Triassic boundary. *Global and Planetary Changes*, **55**, 1–20.

Yin, H.F., Feng, K.L., Baud, A., Xie, S.C., Benton, M.J., Lai, X.L., and Bottjer, D.J. (2007b) The prelude of the end-Permian mass extinction predates a postulated bolide impact. *International Journal of Earth Sciences*, **96**, 903–909.

Ylagan, R.F., Altaner, S.P., and Pozzuoli, A. (2000) Reaction mechanisms of smectite illitization associated with hydrothermal alteration from Ponza island, Italy. *Clays and Clay Minerals*, **48**, 610–631.

(*Received 27 August 2010; revised 31 October 2011; Ms. 479; A.E. H. Dong*)